applied sciences

MDPI

Article

Extraction of the Electromagnetic Parameters of a Metamaterial Using the Nicolson–Ross–Weir Method: An Analysis Based on Global Analytic Functions and Riemann Surfaces

Giovanni Angiulli [1,*,†] and Mario Versaci [2,†]

[1] Department of Information Engineering, Infrastructures and Sustainable Energy, Mediterranea University, 89124 Reggio Calabria, Italy
[2] Department of Civil, Energetic, Environmental and Material Engineering, Mediterranea University, 89124 Reggio Calabria, Italy
* Correspondence: giovanni.angiulli@unirc.it
† These authors contributed equally to this work.

Abstract: The characterization of electromagnetic metamaterials (MMs) plays a fundamental role in their engineering processes. To this end, the Nicolson–Ross–Weir (NRW) method is intensively used to recover the effective parameters of MMs, even though this is affected by the branch ambiguity problem. In this paper, we face this issue in the context of global analytic functions and Riemann surfaces. This point of view allows us to rigorously demonstrate the mathematical foundations of an algorithmic approach for avoiding the branch ambiguity problem, in which the phase unwrapping method is merged with K-K relations for recovering the effective parameters of an MM. In addition, exploiting the intimate relationship between the K-K relations and the Hilbert transform, a simple variant of the above algorithm is presented.

Keywords: metamaterial; Nicolson–Ross–Weir method; phase unwrapping; Kramers–Kronig relations; analytic continuation; global analytic functions; Riemann surfaces

Citation: Angiulli, G.; Versaci, M. Extraction of the Electromagnetic Parameters of a Metamaterial Using the Nicolson–Ross–Weir Method: An Analysis Based on Global Analytic Functions and Riemann Surfaces. *Appl. Sci.* **2022**, *12*, 11121. https://doi.org/10.3390/app122111121

Academic Editor: Xiaojian Fu

Received: 4 October 2022
Accepted: 31 October 2022
Published: 2 November 2022

1. Introduction

Tailoring a material by adjusting its internal microstructure is the key to controlling the interaction between electromagnetic waves and the material itself, i.e., the key to ruling the properties of electromagnetic waves [1]. Electromagnetic metamaterials (MMs) are synthetic composites precisely based on this concept [1–3]. The MM's ability to show exotic properties is due to its intimate structure and based on subwavelength-engineered units called *meta-atoms* [1–3]. However, for analysis and design purposes, an MM is modeled as a continuous medium [1,3]. This viewpoint, called *homogenization procedure* [1,3], allows replacing the detailed description of an electromagnetic MM with a small set of averaged parameters, named *effective parameters* [1–4]. Among the different approaches used for achieving this aim [5,6], the Nicolson–Ross–Weir (NRW) method is the most generally employed because of its theoretical simplicity and ease in algorithmic implementations [7–15]. However, despite the above considerations, it is well known that NRW is affected by some shortcomings that limit the validity of its findings, thus demanding special attention when the effective parameters are retrieved [16,17]. In particular, the *branch ambiguity issue*, i.e., the lack of uniqueness in the evaluation of the effective refractive index, $n_{eff}(\omega)$ [18,19], turns out to be the most critical and problematic of all, even though all the conditions for the employment of the NRW method are fully satisfied [18,19]. In the literature, a number of techniques based on Kramers–Kronig (K-K) relations [20–24] and on the phase unwrapping approach [25–28] have been developed to counter this problem. Concerning the rationale behind the use of K-K relations, it is a direct consequence of the causality principle, which makes it possible to determine the real part of the effective complex refraction

index without any ambiguity, $\mathrm{Re}[N_{eff}(\omega)] = n_{eff}(\omega)$, from the knowledge of its imaginary part, $\mathrm{Im}[N_{eff}(\omega)] = \kappa_{eff}(\omega)$ [29]. Regarding the phase unwrapping approach, its formal equivalence with the operation of analytic continuation of holomorphic functions has been demonstrated very recently in [30]. As clearly shown in [30], the branch ambiguity issue is rooted in the use of the multivalued complex logarithm $LOG(\cdot)$ for solving the NRW relationship. To this aim, an analytic continuation is crucial for performing the proper inversion operation to solve it, thus avoiding any ambiguity in evaluating the effective refractive index $n_{eff}(\omega)$. Starting with the above-mentioned considerations, we extend the analysis conducted in [30], placing the NRW relation in the context of the global analytic functions and the Riemann surfaces. The main results of our study can be summarized as follows: (i) we provide a rigorous mathematical framework within handling the NRW relationship; (ii) we exploit this framework to derive a couple of phase unwrapping-based analytic continuation algorithms, with the first being based on the K-K relations and the second on the Hilbert transform, and they are both capable of solving the NRW equation while avoiding any ambiguity. The idea behind these algorithmic approaches, in the intuitive form, is that the Riemann surface of the global analytic logarithm contains all exact solutions of the NRW equation. More precisely, these solutions are regions of its Riemann surface. Hence, the K-K relations or the Hilbert transform can be used to localize these regions so that the principal complex logarithmic function, appropriately reshaped, can extract the solution of the NRW relationship based on their indications. Furthermore, the theory we propose in this study allows us to rigorously demonstrate some algorithmic procedures empirically proposed in the literature [20,21], broadening their interpretation. The paper is organized as follows: in Section 2, we review the cause of branch ambiguity in the NRW method (Section 2.1) and present a brief discussion on the K-K approach (Section 2.1.1) and the phase unwrapping method (Section 2.1.2) currently used to solve this issue. Afterward, (Section 2.2) we introduce the concept of a global analytic function and Riemann surfaces. First, we discuss the relationship between analytic continuation and global analytic functions (Section 2.2.1) and then the connection between global analytic functions and Riemann surfaces (Section 2.2.2). Finally, we use these theoretical tools to derive a couple of phase unwrapping methods for overcoming the NRW branch ambiguity issue, with the first being based on K-K relations and the second on the Hilbert transform (Section 2.3). In Section 3, their numerical performances are investigated by retrieving the effective refraction index of a couple of hypotetical MM samples and comparing their findings with those provided by the K-K relations and the phase unwrapping approach [30]. In Section 4, conclusions are drawn.

2. Theory

2.1. The Cause of Branch Ambiguity

The Nicolson–Ross–Weir (NRW) method is a well-established procedure first introduced to characterize electromagnetic materials [7] and later employed in the MM field [31]. Using the NRW method, the effective complex refractive index $N_{eff}(\omega)$ of an MM slab with effective thickness d_{eff} is recovered via the inversion of the following relation (the $e^{-i\omega t}$ time convention is assumed and suppressed):

$$e^{iN_{eff}(\omega)k_0 d_{eff}} = \frac{S_{21}(\omega)}{1 - S_{11}(\omega)R_{01}(\omega)} \tag{1}$$

in which k_0, $S_{11}(\omega)$, $S_{21}(\omega)$, and $R_{01}(\omega)$ are, respectively, the free-space propagation constant, scattering parameters, and the reflection coefficient belonging to the effective medium slab related to the MM at hand [30]. Routinely, Equation (1) is solved by using the complex logarithm $LOG(\cdot) = log(\cdot) + 2p\pi i$, where $log(\cdot)$ is the principal logarithm and $p \in \mathbb{Z}$ is the *branch index* [32], from which we obtain, for $\mathrm{Re}[N_{eff}(\omega)] = \kappa_{eff}(\omega)$ and $\mathrm{Im}[N_{eff}(\omega)] = n_{eff}(\omega)$, the following expressions.

$$n_{eff}(\omega) = \frac{1}{k_0 d_{eff}} \mathrm{Im}\left[log\left(\frac{S_{21}(\omega)}{1 - S_{11}(\omega)R_{01}(\omega)}\right)\right] + 2p\pi \tag{2}$$

$$\kappa_{eff}(\omega) = -\frac{1}{k_0 d_{eff}} \mathrm{Re}\left[log\left(\frac{S_{21}(\omega)}{1 - S_{11}(\omega)R_{01}(\omega)}\right)\right] \tag{3}$$

Because of the presence of term p, which ranges in the set of integer numbers, refractive index $n_{eff}(\omega)$ turns out to be not uniquely determined, giving rise to the so-called *branch ambiguity issue* [18,19].

2.1.1. Surmounting the Branch Ambiguity Issue: Kramers–Kronig Relations

Since the effective dielectric permittivity $\epsilon_{eff}(\omega)$ and the effective magnetic permeability $\mu_{eff}(\omega)$ of an MM must be causal quantities [29,33], we have it that their real and imaginary parts must obey Kramers–Kronig (K-K) relations [29,33]. This result suggests a way to overcome the lack of uniqueness afflicting Equation (2). The rationale can be outlined as follows: because of causality, we have it that the effective complex refraction index, $N_{eff}(\omega) = \sqrt{\epsilon_{eff}(\omega)\mu_{eff}(\omega)}$, must be analytic on the complex upper plane $\mathbb{C}^{\uparrow}$, with no zeros on this region [29,33]. This fact allows relating the real and the imaginary part of $N_{eff}(\omega)$ via K-K relations. More precisely, since the term $\kappa_{eff}(\omega)$ is uniquely determined from relation (3), it allows $n_{eff}(\omega)$ to be expressed as follows:

$$n_{eff}(\omega) = 1 + \frac{2}{\pi}\mathcal{P}\int_0^{+\infty} \frac{\omega'\kappa_{eff}(\omega')}{\omega'^2 - \omega^2} d\omega' \tag{4}$$

from which $n_{eff}(\omega)$ can be computed without any ambiguity [30,33]. Exploiting the intimate relationship between K-K relations and the *Hilbert transform:* $\mathcal{H}[\cdot]$

$$\mathcal{H}[\cdot] = \frac{1}{\pi}\mathcal{P}\int_{-\infty}^{+\infty} \frac{[\cdot]}{\omega - \omega'} d\omega' \tag{5}$$

it is possible to rewrite relation (4) as follows [29,34].

$$\mathrm{Re}[N_{eff}(\omega)] = 1 - \mathcal{H}\Big[\mathrm{Im}[N_{eff}(\omega)]\Big] \tag{6}$$

2.1.2. Surmounting the Branch Ambiguity Issue: Phase Unwrapping as Analytic Continuation

As discussed in [30], the branch ambiguity problem afflicting $n_{eff}(\omega)$ is caused by the incorrect handling of Equation (1). Here, we summarize the main theoretical considerations and results from that study. If we set the following:

$$w = iN_{eff}(\omega)k_0 d_{eff} \tag{7}$$

$$z = \frac{S_{21}(\omega)}{1 - S_{11}(\omega)R_{01}(\omega)} \tag{8}$$

relation (1) then becomes

$$e^w = z. \tag{9}$$

Now, if the complex exponential $e^{(\cdot)}$ turns out to be a univalent function [32], it will be invertible, and its inverse will be unique [32]. Accordingly, relation (9) can be solved without ambiguity. However, it has been highlighted in [30] that $e^{(\cdot)}$ holds this property only when the path (8) lies strictly inside a semi-open stright-line strip of $\mathbb{C}$, with width 2π, parallel to $\mathbb{R}^+$. However, since the place where this image lies is tied to $N_{eff}(\omega)$, which is the unknown we are searching for, we must handle $e^{(\cdot)}$ as if it was a non-univalent

function [30]. Therefore, relation (9) can be only *right-inverted* [30,35]; i.e., relation (9) can be solved by evaluating an analytic function $h(\cdot)$ such as the following.

$$e^{(h(z))} = z \quad \forall z \in \mathbb{D} \tag{10}$$

Unlike the inverse function, right-inverse function $h(\cdot)$ is *not unique* [35]. Therefore, when $e^{(\cdot)}$ is handled in this way, it is fundamental to use a suitable constraint condition to obtain a unique solution from inverting Equation (9) (i.e., from inverting (1)) [30]. In [30], it has been demonstrated that $h(\cdot)$ can be computed via an analytic continuation of the principal complex logarithm $log(\cdot)$ on the path traced in $\dot{\mathbb{C}}$ by term (8), which guarantees the fulfillment of condition $\mathrm{Im}(h(0)) = 0$ that ensures the causality of the refractive index [30]. As a further result, in [30], it has been shown that the analytic continuation operation can be carried out by a phase unwrapping method using the algorithm developed by Oppenheim and Schafer for the homomorphic filtering, PUNWOS, [36]. It restores the continuity of the imaginary part of $h(\cdot)$ along path (8) [30], thus unambiguously providing $n_{eff}(\omega)$ as follows.

$$n_{eff}(\omega) = \frac{1}{k_0 d_{eff}} \mathrm{Im}[h(z)] \tag{11}$$

2.2. Analytic Continuation, Global Analytic Functions, and Riemann Surfaces

In this section, we will introduce the theoretical concepts of the global analytic function and Riemann surface. Using these mathematical tools, the K-K and phase unwrapping approaches can be *merged together*, thus providing an analytic continuation algorithmic methodology to solve Equation (1). Roughly speaking, the rationale is the following: In [30], it was shown that the solution of Equation (9) is given by the analytic continuation of the principal complex logarithm over the domain defined by the path described by Equation (8). Hence, different solutions of Equation (9) correspond to different analytic function elements. At this stage, the idea to exploit the global analytic functions and Riemann surface has its origin. A global analytic function is a pool containing all analytic continuations of its essential components—the analytic function elements, i.e., precisely the objects that are solutions of Equation (9). Accordingly, in Section 2.2.1, we will show that the set of all solutions of Equation (9) realizes the global analytic logarithm. In Section 2.2.2, we will discuss the concepts of Riemann surfaces and the lift operation (or lifting operation). We will show how the Riemann surface for the global analytic logarithm is realized by the Cartesian product between solutions of Equation (9) and points of the complex plane and how the lifting operation allows placing, in correspondence, the values assumed by the global analytic logarithm on regions of the Riemann surface with the values taken by the solution of Equation (9) on its domain of definition, i.e, the path (8). From this fundamental relation, we derive an algorithmic approach to solve Equation (9) in which the phase unwrapping method (i.e., the analytic continuation) is merged with the K-K relations and a variant based on the Hilbert transform. All topics will be presented in-depth, although topological details will be omitted to simplify the discussion.

2.2.1. Analytic Continuation and Global Analytic Functions

Roughly speaking, the analytic continuation is the operation with which it is possible to enlarge the domain of an analytic function $f(\cdot)$, Ω. To formalize this idea, we provide the following definition [32].

Definition 1. *An ordered pair $(\Omega, f(\cdot))$ where Ω is a domain ($\Omega \subset \mathbb{C}$) and $f(\cdot)$ is an analytic function is called an analytic function element. A pair $(\Omega_N, f_N(\cdot))$ is the direct analytic continuation of a pair $(\Omega_1, f_1(\cdot))$ if the following is the case.*

$$f_1(z) = f_N(z) \quad \forall z \in \Omega_1 \cap \Omega_N \quad (\Omega_1 \cap \Omega_N \neq \varnothing) \tag{12}$$

Alternatively, they are indirect analytic continuations of each other if the following set of analytic function elements exist between elements $(\Omega_1, f_1(\cdot))$ *and* $(\Omega_N, f_N(\cdot))$*:*

$$\{(\Omega_2, f_2(\cdot)), \ldots, (\Omega_{N-1}, f_{N-1}(\cdot))\} \tag{13}$$

where $(\Omega_k, f_k(\cdot))$ *is the direct analytic continuation of* $(\Omega_{k-1}, f_{k-1}(\cdot))$ *for* $k = 2, \ldots, N$ *[32].*

Based on the above statements, a global analytic function $\mathcal{G}$ is a non-empty set of pairs $(\Omega, f(\cdot))$ that are the direct or indirect analytic continuation of each other [32,35].The union $\mathbb{M} = \cup_i \Omega_i$ of all domains Ω_i of all analytic function elements belonging to $\mathcal{G}$ is the domain of existence of $\mathcal{G}$ [32]. Each analytic function elements $(\Omega, f(\cdot)) \in \mathcal{G}$ is called a *branch* of $\mathcal{G}$ [35]. The value w_0 provided by a pair $(\Omega, f(\cdot)) \in \mathcal{G}$ at $z_0 \in \Omega$, i.e., $w_0 = f(z_0)$, is called the value of $\mathcal{G}$ at z_0 [32]. A global analytic function $\mathcal{G}$ can have several branches over the same domain. This behavior follows directly from the indirect analytic continuation's working, which can provide different results using different sequences of analytic function elements [32,35]. In that case, $\mathcal{G}$ is a multivalued function from $\mathbb{M}$ to $\mathbb{C}$ [32,35].

Remark 1. *The set* $\mathcal{L}$ *of all analytic function elements* $(\Omega, h(\cdot))$ *for which the following equation*

$$e^{h(z)} = z \quad \forall z \in \Omega \tag{14}$$

holds is a global analytic function, $\mathcal{L}$*, and is named the global analytic logarithm [32]. Its domain of existence is* $\mathbb{M} = \dot{\mathbb{C}}$*. Any branch of* $\mathcal{L}$ *has the form* $log(\cdot) = ln|\cdot| + i[arg_\pi(\cdot)]$*, where* $ln|\cdot|$ *and* $arg_\pi(\cdot)$ *are the natural logarithm of the absolute value function and the principal argument function, respectively. Two distinct branches of* $\mathcal{L}$ *differ by* $2p\pi i$ *where* $p \in \mathbb{Z}$ *[32,35].*

2.2.2. Global Analytic Functions and Riemann Surfaces

To handle a multivalued global analytic function $\mathcal{G}$ as a function in the ordinary sense, it becomes mandatory to redefine a suitable domain $\mathbb{S}(\mathcal{G})$ for $\mathcal{G}$ and to operate in a way that it becomes an ordinary single-valued function from the new domain $\mathbb{S}(\mathcal{G})$ to $\mathbb{C}$. To this aim, instead of dealing with analytic function elements $(\Omega, f(\cdot))$, where Ω is an arbitrary domain, we have to consider pairs of the form $(\Delta, f(\cdot))$ where $\Delta \subseteq \Omega$ is a disk [35]. Between these elements, it is possible to introduce an equivalence relation [35,37].

Definition 2. *Two pairs* $(\Delta', f'(\cdot))$ *and* $(\Delta'', f''(\cdot))$*, with disks* Δ' *and* Δ'' *centered in* z' *and* z''*, respectively, are equivalent if the following is the case:*

$$(z' = z'') \wedge (f'(\cdot) = f''(\cdot)) \tag{15}$$

in some neighborhood of the point z'*.*

From it, we derive the possibility to partition $\mathcal{G}$ into particular subsets, called *germs* [37].

Definition 3. *The set of all the equivalent pairs* $(\Delta, f(\cdot)) \in \mathcal{G}$ *is called germ, centered at* z*, and denoted by the symbol* $[f]_z$*. The value of a germ* $[f]_z$ *at its center* z*,* $[\bar{f}]_z$*, is the value* $w = f(z)$ *given by any of its elements at* z*.*

The germs can be collected together as sets [37].

Definition 4. *The set of all germs in which all elements* $(\Delta, f(\cdot))$ *belonging to a global analytic function* $\mathcal{G}$ *can be collected is denoted by* $\mathcal{G}^*$*. The set of all germs in* $\mathcal{G}^*$ *with the same center* z *is denoted by* $\mathcal{G}^*_z$*.*

Using the concept of a set of germs, we can introduce a theorem that formalizes what was first said about the number of values that a global analytic function $\mathcal{G}$ could assume

in correspondence to a given point z of its domain of existence $\mathbb{M}$ (for its demonstration, see [32]).

Theorem 1 (Poincaré–Volterra). *Let $\mathcal{G}$ be a global analytic function. For all $z \in \mathbb{C}$ and $\mathcal{G}_z^* \in \mathcal{G}^*$, the cardinality of $\mathcal{G}_z^*$ is at most countable.*

Based on the Poincaré-Volterra theorem, we are in the condition to introduce the concept of Riemann surface $\mathbb{S}(\mathcal{G})$ for a global analytic function $\mathcal{G}$. It consists of a number of *abstract sheets* lying above $\mathbb{C}$. These sheets (or layers) can be built by associating an array to each $z \in \mathbb{C}$, for which its elements are germs belonging to set $\mathcal{G}_z^*$ with the center at z. The array can be empty (no germs at all) or, at most, have an infinite (countable) dimension [35,37]. In a more formal language, we have the following.

Definition 5. *The set*

$$\mathbb{S}(\mathcal{G}) = ((z, [f]_z) : z \in \mathbb{C}, [f]_z \in \mathcal{G}_z^*) \tag{16}$$

is the Riemann surface related to $\mathcal{G}$.

Remark 2. *In the case of the global analytic logarithm $\mathcal{L}$, its Riemann surface $\mathbb{S}(\mathcal{L})$ is realized by all pairs $(z, [f]_z)$ where $z \in \dot{\mathbb{C}}$ and $[f]_z = log(\cdot) + 2p\pi i$ where $p \in \mathbb{Z}$. The p-th sheet of $\mathbb{S}(\mathcal{L})$, $\mathbb{S}_p(\mathcal{L})$, consists of all couples of $(z, log(\cdot) + 2p\pi i)$ with p fixed.*

In other words, $\mathbb{S}(\mathcal{G})$ is a subset of the Cartesian product between $\mathbb{C}$ and $\mathcal{G}$. Using the Riemann surface $\mathbb{S}(\mathcal{G})$ in lieu of $\mathbb{M}$, it is possible to redefine $\mathcal{G}$ in a way that it realizes a function from its Riemann surface $\mathbb{S}(\mathcal{G})$ to $\mathbb{C}$ [37].

Definition 6. *The function $\hat{\mathcal{G}}[\cdot]$ is as follows:*

$$\hat{\mathcal{G}}[(z, [f]_z)] = w \quad (z, [f]_z) \in \mathbb{S}(\mathcal{G}), w \in \mathbb{C}, \tag{17}$$

where $w = [\bar{f}]_z$ is called the lift of $\mathcal{G}$ on its Riemann surface $\mathbb{S}(\mathcal{G})$.

Another function of paramount importance is the following.

Definition 7. *The function $\hat{\mathcal{P}}[\cdot]$*

$$\hat{\mathcal{P}}[(z, [f]_z)] = z \quad (z, [f]_z) \in \mathbb{S}(\mathcal{G}), z \in \mathbb{C} \tag{18}$$

is called the projection of $\mathbb{S}(\mathcal{G})$ to $\mathbb{C}$.

To clarify the idea behind the lift operation, let us consider set $\hat{\Omega}$ of all pairs $(z, [f]_z)$ such that $z \in \bar{\Omega}$, and $[f]_z$ is germ-derived by $(\bar{\Omega}, \bar{f}(\cdot))$. This set, $\hat{\Omega}$, is a copy of Ω on $\mathbb{S}(\mathcal{G})$ (we recall that $\hat{\mathcal{P}}[(z, [f]_z)] = z \in \bar{\Omega}$). Let $(z, [f]_z)$ be an element of $\hat{\Omega}$; then, according to definition (6), we have the following.

$$\hat{\mathcal{G}}[(z, [f]_z)] = [\bar{f}]_z = \bar{f}(z) \tag{19}$$

In otherwords, $\hat{\mathcal{G}}[\cdot]$ assigns to each point in $(z, [f]_z) \in \hat{\Omega} \subset \mathbb{S}(\mathcal{G})$ precisely the same value that $\bar{f}(\cdot)$ assigns to each point in $z \in \bar{\Omega} \subset \mathbb{C}$. In sum, we have that the lift of $\mathcal{G}$ on its Riemann surface, $\hat{\mathcal{G}}[\cdot]$, and it is restricted to $\hat{\Omega}$ and behaves exactly as $\bar{f}(\cdot)$ on $\bar{\Omega}$ [37].

Remark 3. *The lift of $\mathcal{L}$ on $\mathbb{S}(\mathcal{L})$ is given by the following.*

$$\hat{\mathcal{L}}[(z, [f]_z])] = [\bar{f}]_z = log(z) + 2p\pi i \tag{20}$$

If $(\Omega, f(\cdot)) \in \mathcal{L}$, *the set* $\hat{\Omega}$ *of all pairs*

$$(z, log(\cdot) + 2p\pi i), \quad z \in \Omega \tag{21}$$

is a copy of Ω *on* $\mathbb{S}(\mathcal{L})$. *The integers* p *fulfilling Equation (21) define sheets* $\mathbb{S}_p(\mathcal{L})$ *where* $\hat{\Omega}$ *lies.*

2.3. Kramers–Kronig Relations and Phase Unwrapping Approach: A Unique Point of View within the Framework of the Global Analytic Functions on Riemann Surfaces

As stated in Sections 2.1.1 and 2.1.2, Equation (1) is solved by evaluating $h(\cdot)$ via the K-K relations or by the phase unwrapping approach, and both methods are equivalent to analytic continuation. It is quite straightforward to encompass these methods in the theoretical framework given in Section 2.2.2. Specifically, from Remark 1, the set of all the solutions of Equation (9) is a global analytic function, i.e, the global analytic logarithm $\mathcal{L}[\cdot]$; from Remark 2, we have the explict structure of its Riemann surface $\mathbb{S}(\mathcal{L})$; finally, from Remark 3, the values assumed by the lift of the global analytic logarithm $\hat{\mathcal{L}}[(\cdot)]$ on sub-domain $\hat{\mathbb{D}}$ established by pairs $(z, [f]_z])$ are *equal* to the values taken by $h(\cdot)$ on $\mathbb{D}$; i.e., between the lift of global analytic logarithm, $\hat{\mathcal{L}}[\cdot]$, and the right inverse $h(\cdot)$, relation (20) must hold.

$$\hat{\mathcal{L}}[(z, [f]_z])] = [\bar{f}]_z = h(z) \quad \forall z \in \mathbb{D} \tag{22}$$

That is, we have the following.

$$[\bar{f}]_z = log(z) + 2p\pi i = h(z) \quad \forall z \in \mathbb{D} \tag{23}$$

Only in the context of the theory described above can the equalities (22) and (23) be derived and have meaning. Since $log(\cdot) = ln|\cdot| + i[arg_\pi(\cdot)]$, we can write the following.

$$\mathsf{Im}[h(z)] = [arg_\pi(z) + 2p\pi] = \quad \forall z \in \mathbb{D} \tag{24}$$

Considering Equation (8), the above relation can be written as follows.

$$\mathsf{Im}\left[h\left(\frac{S_{21}(\omega)}{1 - S_{11}(\omega)R_{01}(\omega)}\right)\right] = \left[arg_\pi\left(\frac{S_{21}(\omega)}{1 - S_{11}(\omega)R_{01}(\omega)}\right) + 2p\pi\right] \tag{25}$$

With respect to integers p that specify the sheets of $\mathbb{S}(\mathcal{L})$ where $(\mathbb{D}, h(\cdot))$ is embedded, they are unknowns that have to be determined. By means of Equation (11), we can write Equation (25) as follows.

$$k_0 d_{eff} n_{eff}(\omega) = \left[arg_\pi\left(\frac{S_{21}(\omega)}{1 - S_{11}(\omega)R_{01}(\omega)}\right) + 2p\pi\right] \tag{26}$$

Because term $n_{eff}(\omega)$ can be obtained from $\kappa_{eff}(\omega)$ via the K-K relation (4), p can be evaluated as follows.

$$p = \frac{1}{2\pi}\left[k_0 d_{eff}\left(1 + \frac{2}{\pi}\mathcal{P}\int_0^{+\infty} \frac{\omega'\kappa_{eff}(\omega')}{\omega'^2 - \omega^2} d\omega'\right) - arg_\pi\left(\frac{S_{21}(\omega)}{1 - S_{11}(\omega)R_{01}(\omega)}\right)\right] \tag{27}$$

Equation (25) highlights an important concept: $\mathsf{Im}[h(\cdot)]$ can be determined from the knowledge of the argument of the principal logarithm, $arg_\pi(\cdot)$, properly compensated by phase term $2p\pi$, where unknown integer p can be evaluated by using K-K relations by using Equation (27). Once we determined $\mathsf{Im}[h(\cdot)]$, the effective refractive index $n_{eff}(\omega)$ can be evaluated via Equation (11). In sum, using the framework of global analytic functions, we rigorously demonstrated and derived a phase unwrapping approach based on Kramers–Kronig relations, which provides an analytic continuation solution $h(\cdot)$ for Equation (1) based on $log(\cdot)$ and restoring the continuity of its imaginary part, $\mathsf{Im}[h(\cdot)]$ [30], given by

$arg_\pi(\cdot)$. As an alternative, using the Hilbert transform of $\kappa_{eff}(\omega)$ from Equation (5), we have the following.

$$p = \frac{1}{2\pi}\left[k_0 d_{eff}\left(1 - \mathcal{H}(\kappa_{eff}(\omega))\right) - arg_\pi\left(\frac{S_{21}(\omega)}{1 - S_{11}(\omega)R_{01}(\omega)}\right)\right] \tag{28}$$

3. Results

As derived in the above section, relations (27) and (28) represent two phase unwrapping approaches based on the K-K relation (4) and the Hilbert transform (6), respectively. We named PUNW$_{KK}$ and PUNW$_{HT}$ the related numerical procedures. Regarding the PUNW$_{KK}$ method, the numerical evaluation of the involved K-K integral has been performed using the Simpson quadrature method described in [38], while for the PUNW$_{HT}$ procedure, the Hilbert Transform has been computed by using the FFT technique described in [34]. For both methods, the parameter p has been determined, forcing it to assume an integer value selected to ensure the continuity of $arg_\pi(\cdot)$ [36]. To assess their numerical performances, we compared these with those provided by the numerical evaluation of the K-K relation (4) using the same numerical integration algorithm adopted for PUNW$_{KK}$ [38] and the phase unwrapping PUNWOS method [36] using the implementation described in [30]. To this end, we have considered recovering the effective refractive index $n_{eff}(\omega)$ of two theoretical double negative MM slabs, in which relative permeability $\mu_r(\omega)$ and permittivity $\epsilon_r(\omega)$ are described by the following Lorentzian model [3].

$$\mu_r(\omega) = \mu_\infty + \sum_{n=1}^{np} \frac{(\mu_{s,n} - \mu_\infty)\omega_{0m,n}^2}{\omega_{0m,n}^2 - \omega^2 + i\gamma_{m,n}\omega} \tag{29}$$

$$\epsilon_r(\omega) = \epsilon_\infty + \sum_{n=1}^{np} \frac{(\epsilon_{s,n} - \epsilon_\infty)\omega_{0e,n}^2}{\omega_{0e,n}^2 - \omega^2 + i\gamma_{e,n}\omega} \tag{30}$$

The parameters of the two models are reported in Table 1. This modeling choice is justified because: (*i*) Lorentzian models describe the dispersive nature of split-ring resonators and strip wires [3], and (*ii*) the superposition of Lorentzian functions describes every causal function [39]. The MATLAB environment has been employed to code all methods. All numerical experiments were performed on a 2.0 GHz Intel Xeon workstation. The percentage error (PE) is defined as follows:

$$\frac{\|n_{ex}(\omega) - n_{eff}(\omega)\|_2}{\|n_{ex}(\omega)\|_2}\% \tag{31}$$

where $\|\cdot\|_2$ is the 2-norm [40], $n_{ex}(\omega) = \mathrm{Re}[\sqrt{\epsilon_r(\omega)\mu_r(\omega)}]$ and $n_{eff}(\omega)$ are the exact and recovered refractive indexes, respectively, which have been used as criteria to evaluate the efficiency of the considered recovering procedures. Moreover, computational time t has been evaluated. However, this last datum has to be considered as only indicative of the order of magnitude rather than the exact time involved in each considered retrieval procedure since such knowledge would require the development of numerical codes optimized for a given CPU in order to achieve the best possible computational performances [41]. Figure 1 shows path $\gamma(\omega)$ traced by Equation (8) for the first slab, with $d_{eff} = 180$ nm, which is characterized by a single pole Lorentzian model for pair $(\epsilon_r(\omega), \mu_r(\omega))$. As pointed out in [30], this trend for $\gamma(\omega)$ confirms that this is an electrically thick slab because $\gamma(\omega)$ repeatedly intersects ray $\mathbb{R}_\pi$, i.e., the branch cut for the principal complex logarithm $log(\cdot)$ [30,32]. Accordingly, the complex exponential function in equation $e^{(\cdot)}$ in (1) lacks univalence for the considered case, thus indicating that $n_{eff}(\omega)$ must be evaluated via the right-inverse operation [30]. Table 2 shows the values of PE and t as a function of the number of sample points n_s in frequency band $[0, 1]$ PHz for all the considered recovering methods.

Table 1. Parameters for the Lorentzian model adopted in this study.

	First slab: $np = 1$, $d_{eff} = 180$ nm		
ϵ_∞	1.8	μ_∞	1.0
$\epsilon_{s,1}$	2.0	$\mu_{s,1}$	1.3
$\omega_{oe,1}$	2π·0.695 PHz	$\omega_{om,1}$	2π·0.7 PHz
$\gamma_{e,1}$	0.08 PHz	$\gamma_{m,1}$	0.05 PHz
	Second slab: $np = 2$, $d_{eff} = 300$ nm		
ϵ_∞	1.8	μ_∞	1.0
$\epsilon_{s,1}$	2.5	$\mu_{s,1}$	1.8
$\epsilon_{s,2}$	2.0	$\mu_{s,1}$	1.3
$\omega_{oe,1}$	2π·0.695 PHz	$\omega_{om,1}$	2π·0.7 PHz
$\omega_{oe,2}$	2π·0.895 PHz	$\omega_{om,2}$	2π·0.899 PHz
$\gamma_{e,1}$	0.09 PHz	$\gamma_{m,1}$	0.07 PHz
$\gamma_{e,2}$	0.08 PHz	$\gamma_{m,2}$	0.05 PHz

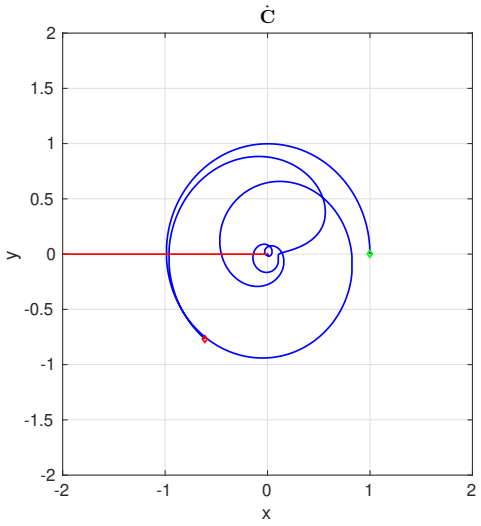

Figure 1. Path $\gamma(\omega)$ traced by Equation (8) on the complex punctured plane $\dot{\mathbb{C}}$ for the slab with $d_{eff} = 180$ nm. Green diamond marker: path starting point, $\omega = 0$ Hz. Red diamond marker: path end point, $\omega = 1$ PHz.

Table 2. Percentage Error (PE) and computational time t for the slab with $d_{eff} = 180$ nm.

n_s	**PE** PUNWOS	K-K	PUNW$_{KK}$	PUNW$_{HT}$
512	303.88	13.97	1.51×10^{-3}	1.51×10^{-3}
1024	260.49	13.67	1.11×10^{-3}	1.11×10^{-3}
2048	130.14	13.61	2.63×10^{-3}	2.63×10^{-3}
4096	2.01×10^{-3}	13.63	2.01×10^{-3}	2.01×10^{-3}
n_s	***t*** (s) PUNWOS	K-K	PUNW$_{KK}$	PUNW$_{HT}$
512	0.25	0.29	0.35	0.34
1024	0.28	0.42	0.34	0.33
2048	0.26	1.01	0.54	0.69
4096	0.33	2.92	1.16	0.35

In correspondence to starting value $n_s = 512$, we can note that the PE value turns out to be high for the K-K approach and very high for the PUNWOS method, whereas

in the cases of the PUNW$_{KK}$ and PUNW$_{HT}$ methods, it is already factually negligible. In correspondence to $n_s = 1024$, the value of this parameter related to the PUNW$_{HT}$ and the PUNW$_{KK}$ methods is still factually insignificant, whereas in the cases of the PUNWOS and K-K methods, it turns out to be comparable to the previous case. While increasing to $n_s = 2048$, the above trend remains stationary for all methods. Finally, for $n_s = 4096$, we have three unwrapping methods (PUNWOS, PUNW$_{KK}$ and PUNW$_{HT}$) that provide a factually insignificant PE, whereas we have no improvements for the PE in the case of the K-K method. As indicated by the PE parameter, values reported in Table 2 are confirmed by the results shown in Figure 2, which reports the plot of the retrieved refractive index $n_{eff}(\omega)$ compared with the exact refractive index $n_{ex}(\omega)$ for the four recovering methods for all the considered n_s values. Figure 3 shows the sequence of p integers needed to give continuity to $arg_\pi(\cdot)$ provided by PUNWOS, PUNW$_{HT}$, and PUNW$_{KK}$ for $n_s = 2048$. The high PE related to the PUNWOS method is clearly due to its incorrect calculation of the p sequence until an adequate number of sample points n_s is used. Figure 4 shows path $\gamma(\omega)$ traced by Equation (8) for the slab with $d_{eff} = 300$ nm. This last case we analyzed is characterized by a double pole Lorentzian model for its pair $(\epsilon_r(\omega), \mu_r(\omega))$. Since for this slab, the resulting path $\gamma(\omega)$ intersects $\mathbb{R}_\pi$ many times more than in the previously considered case, the number of integers p that has to be computed to recover the continuity of $arg_\pi(\cdot)$ will be higher than previously performed, thus providing a more challenging test for the considered recovering approaches. The results reported in Table 3 validate the above hypothesis. For this test case, only the PUNW$_{HT}$ method provides values for PE that are factually negligible for all considered values of n_s. Lower performances characterize all other remaining methods. More precisely, the PUNWOS method reaches a value of PE equal to those characterizing PUNW$_{HT}$ only when the number of sample point in the $[0, 1.5]$ PHz band increases to $n_s = 16{,}384$. On the other hand, for K-K and PUNW$_{KK}$ methods, the PE is always high, thus providing a recovered $n_{eff}(\omega)$ of lower quality, as demonstrated by the results reported in Figure 5, which shows the plot of $n_{eff}(\omega)$ compared with $n_{ex}(\omega)$, as a function of n_s over the $[0, 1.5]$ PHz frequency range. The results shown in Figure 6 confirm what has been stated about the number of p integers needed to ensure the continuity of the argument of $log(\cdot)$, meaning that the number of Riemann sheets involved by $h(\cdot)$ increase (as expected) with an increase in the slab's thickness. Moreover, in this case, the high PE related to the PUNWOS method is clearly due to its incorrect calculation of the p sequence until an adequate number of sample points n_s is used.

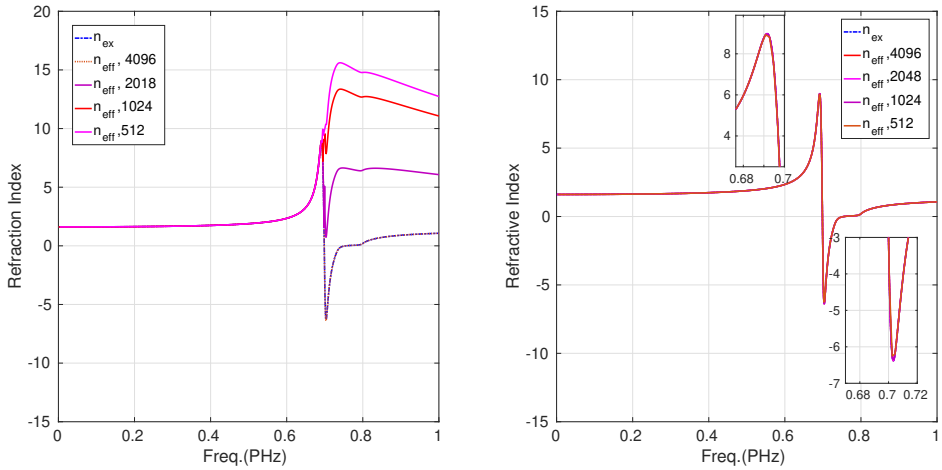

Figure 2. *Cont.*

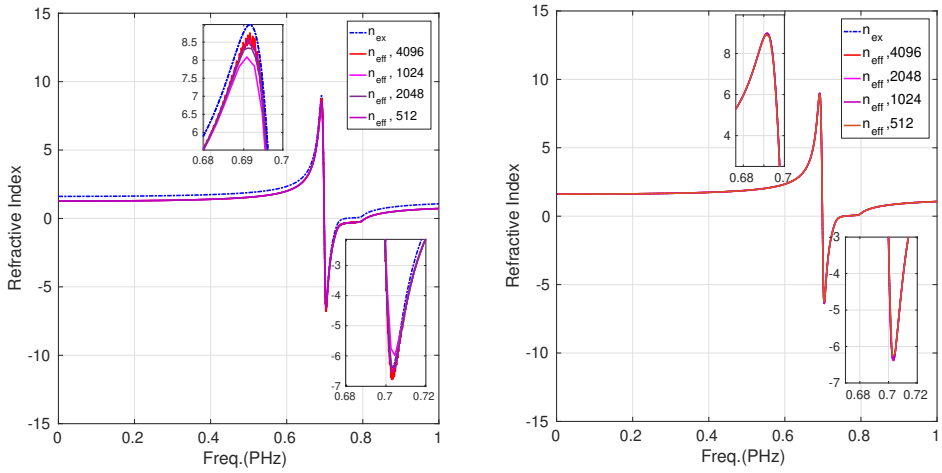

Figure 2. Plot of $n_{eff}(\omega)$, as a function of n_s, and $n_{ex}(\omega)$ for the MM with $d_{eff} = 180$ nm over the frequency band $[0, 1]$ PHz. **Top left**: PUNWOS method; **top right**: PUNW$_{HT}$ method; **bottom left**: K-K relations; **bottom right**: PUNW$_{KK}$ method. The insets magnify $n_{eff}(\omega)$ around its peaks.

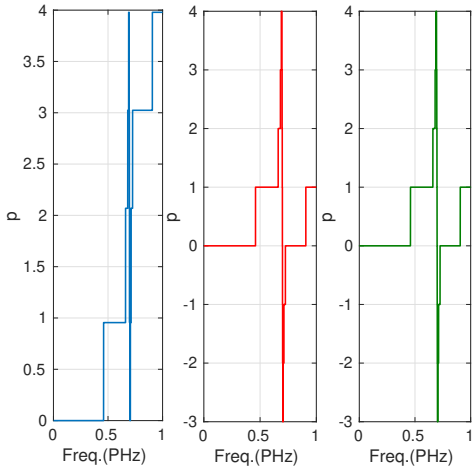

Figure 3. Values of the integer p over the band $[0, 1]$ PHz ($n_s = 2048$). **Left**: PUNWOS; **centre**: PUNW$_{HT}$; **right**: PUNW$_{KK}$.

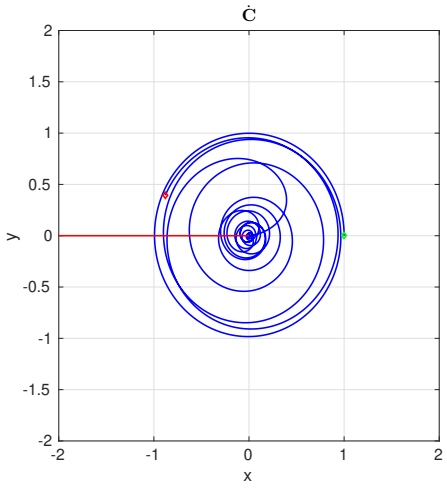

Figure 4. Path $\gamma(\omega)$ traced by (8) on the complex punctured plane $\dot{\mathbb{C}}$ for the slab with $d_{eff} = 300$ nm. Green diamond marker: path starting point, $\omega = 0$ Hz. Red diamond marker: path end point, $\omega = 1.5$ PHz.

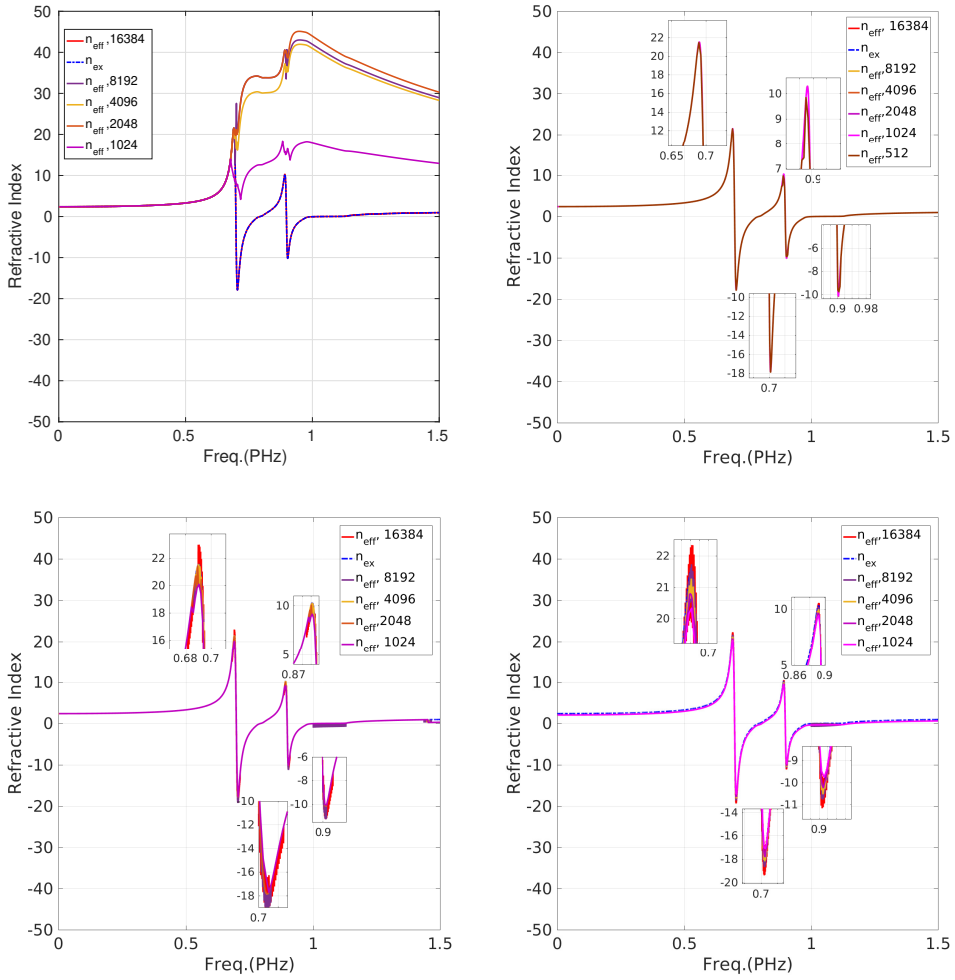

Figure 5. Plot of $n_{eff}(\omega)$, as a function of n_s and $n_{ex}(\omega)$ for the MM with $d_{eff} = 300$ nm over frequency band $[0, 1.5]$ PHz. **Top left**: PUNWOS method; **top right**: PUNW$_{HT}$ method; **bottom left**: K-K relations; **bottom right**: PUNW$_{KK}$ method. The insets magnify $n_{eff}(\omega)$ around its peaks.

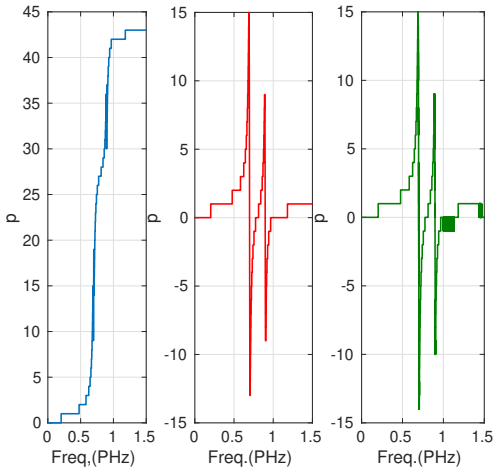

Figure 6. Values of the integer p over the $[0, 1.5]$ PHz ($n_s = 8196$). **Left**: PUNWOS; **centre**: PUNW$_{HT}$; **right**: PUNW$_{KK}$.

Table 3. Percentage error (PE) and computational time t for the slab with $d_{eff} = 300$ nm.

n_s	PE PUNWOS	K-K	PUNW$_{KK}$	PUNW$_{HT}$
1024	206.03	6.86	3.90	5.76×10^{-4}
2048	503.37	6.51	3.19	5.62×10^{-4}
4096	464.54	6.48	2.84	5.81×10^{-4}
8192	485.42	6.72	3.93	7.73×10^{-4}
16,384	8.85×10^{-4}	6.86	3.86	8.85×10^{-4}
n_s	t (s) PUNWOS	K-K	PUNW$_{KK}$	PUNW$_{HT}$
1024	0.30	0.41	0.37	0.36
2048	0.31	0.93	0.50	0.37
4096	0.38	3.18	1.30	0.27
8192	0.40	11.13	3.84	0.35
16,384	0.37	45.04	14.97	0.33

4. Conclusions

In this work, we extend the analysis conducted in [30], placing the NRW relation in the context of the global analytic functions and the Riemann surfaces, thus providing a rigorous mathematical framework for handling the NRW relationship. In this context, the branch ambiguity problem finds its correct interpretation in terms of the number of Riemann surface sheets $\mathbb{S}(\mathcal{L})$ on which the right-inverse $h(\cdot)$, the solution of the NRW Equation (1), lies. Furthermore, we exploit this framework to derive a couple of phase unwrapping-based analytic continuation algorithms: the first, named PUNW$_{KK}$, is based on K-K relations, and the second, named PUNW$_{HT}$, is based on the Hilbert transform; both are capable of solving the NRW equation and avoid any ambiguity. To validate their numerical performances, some numerical experiments conducted on a couple of theoretical negative refractive index (NRI) slabs have been carried out. The close agreement obtained between the recovered and the exact refraction index provided by the PUNW$_{HT}$ approach demonstrates its superiority over the other recovery methods considered in this study and confirms the validity of our theoretical analyses. Although the results provided by the PUNW$_{KK}$ were less satisfactory than those given by PUNW$_{HT}$, the use of K-K relations merged with the phase unwrapping approach enhances the results these relations provides. Finally, to conclude, we point out that the theory we have given in this work rigorously demonstrates some algorithmic procedures empirically proposed in the literature [20,21], broadening their meaning.

Author Contributions: Conceptualization, G.A.; methodology, G.A. and M.V.; software, G.A.; validation, M.V.; formal analysis, G.A.; investigation, G.A. and M.V.; resources, M.V.; writing—original draft preparation, G.A. and M.V. All authors have read and agreed to the published version of the manuscript.

Funding: This research received no external funding.

Institutional Review Board Statement: Not applicable.

Informed Consent Statement: Not applicable.

Data Availability Statement: Not applicable.

Conflicts of Interest: The authors declare no conflicts of interest.

Abbreviations

The following symbols are used in this manuscript:

$LOG(\cdot)$	Complex logarithm;
$log(\cdot)$	Principal logarithm;
$ln(\cdot)$	Natural logarithm function;
$\lvert\cdot\rvert$	Absolute value function;
$arg_\pi(\cdot)$	Principal argument function;
p	Branch index;
$e^{(\cdot)}$	Complex exponential;
$h(\cdot)$	Right inverse function;
$\mathcal{H}[\cdot]$	Hilbert transform;
$\mathcal{P}$	Cauchy principal value;
$\mathbb{C}$	Complex plane;
$\dot{\mathbb{C}}$	Complex punctured plane;
$\mathbb{R}^+$	Positive real axis;
$\mathbb{C}^\uparrow$	Upper complex plane;
$\mathcal{G}$	A global analytic function;
$[f]_z$	Germ centered at z;
$[\bar{f}]_z$	Value of the germ at z;
$\mathcal{G}^*$	Set of all the germs $[f]_z$ of $\mathcal{G}$;
$\mathcal{G}_z^*$	Set of all the germs $[f]_z$ centered at z;
$\mathbb{M}$	Domain of existence of a global analytic functionv
$\mathcal{L}$	Global analytic logarithm;
$\hat{\mathcal{L}}[\cdot]$	Lift of the global analytic logarithm;
$\mathbb{S}(\mathcal{G})$	Riemann surface of $\mathcal{G}$;
$\hat{\mathcal{G}}[\cdot]$	Lift of $\mathcal{G}$ on $\mathbb{S}(\mathcal{G})$;
$\hat{\mathcal{P}}[\cdot]$	Projection from the Riemann surface $\mathbb{S}(\mathcal{G})$ to $\mathbb{C}$.

References

1. Xiaojian, F.; Cui, T.-J. Recent progress on metamaterials: From effective medium model to real-time information processing system. *Prog. Quantum Electron.* **2019**, *67*, 100223.
2. Padilla, W.J.; Averitt, R.D. Imaging with metamaterials. *Nat. Rev. Phys.* **2022**, *4*, 85–100. [CrossRef]
3. Cui, T.J.; Smith, D.R.; Liu, R. *Metamaterials*; Springer: Berlin/Heidelberg, Germany, 2010.
4. Cui, T.J.; Tang, W.X.; Yang, X.M.; Mei, Z.L.; Jiang, W.X. *Metamaterials: Beyond Crystals, Noncrystals, and Quasicrystals*; CRC Press: Boca Raton, FL, USA, 2017.
5. Smith, D.R.; Pendry, J.B. Homogenization of metamaterials by field averaging. *JOSA B* **2006**, *23*, 391–403. [CrossRef]
6. Alú, A. First-principles homogenization theory for periodic metamaterials. *Phys. Rev. B* **2011**, *84*, 075153. [CrossRef]
7. Chen, L.F.; Ong, C.K.; Neo, C.P.; Varadan, V.V.; Varadan, V.K. *Microwave Electronics: Measurement and Materials Characterization*; John Wiley & Sons: Hoboken, NJ, USA, 2004.
8. Ujan, R.; Bahadur, A.; Shabir, G.; Iqbal, S.; Saeed, A.; Channar, P.A.; Mahmood, Q.; Shoaib, M.; Arshad, I.; Saifullah, M.; et al. Facile synthesis of novel fluorescent thiazole coumarinyl compounds: Electrochemical, time resolve fluorescence, and solvatochromic study. *J. Mol. Struct.* **2021**, *1227*, 129422. [CrossRef]
9. Bahadur, A.; Iqbal, S.; Ujan, R.; Channar, P.A.; AL-Anazy, M.M.; Saeed, A.; Mahmood, Q.; Shoaib, M.; Shah, M.; Arshad, I.; et al. Effect of organic solvents on solvatochromic, fluorescence, and electrochemical properties of synthesized thiazolylcoumarin derivatives. *Luminescence* **2021**, *36*, 1189–1197. [CrossRef]
10. Hakim, M.L.; Alam, T.; Islam, M.T.; Baharuddin, M.H.; Alzamil, A.; Islam, M.S. Quad-Band Polarization-Insensitive Square Split-Ring Resonator (SSRR) with an Inner Jerusalem Cross Metamaterial Absorber for Ku-and K-Band Sensing Applications. *Sensors* **2022**, *22*, 4489. [CrossRef]
11. Idrus, I.N.; Faruque, M.R.I.; Abdullah, S.; Khandaker, M.U.; Tamam, N.; Sulieman, A.A. An Oval-Square Shaped Split Ring Resonator Based Left-Handed Metamaterial for Satellite Communications and Radar Applications. *Micromachines* **2022**, *13*, 578. [CrossRef]
12. Sgró, A.; De Carlo, D.; Angiulli, G.; Morabito, F.C.; Versaci, M. Accurate computation of Drude-Lorentz model coefficients of single negative magnetic metamaterials using a micro-genetic algorithm approach. In *Multidisciplinary Approaches to Neural Computing*; Springer: Cham, Switzerland, 2018; pp. 47–55.
13. Hannan, S.; Islam, M.T.; Almutairi, A.F.; Faruque, M.R.I. Wide bandwidth angle-and polarization-insensitive symmetric metamaterial absorber for X and Ku band applications. *Sci. Rep.* **2020**, *10*, 10338 . [CrossRef]

14. Ajewole, B.; Kumar, P.; Afullo, T. I-Shaped Metamaterial Using SRR for Multi-Band Wireless Communication. *Crystals* **2022**, *12*, 559. [CrossRef]
15. Islam, M.R.; Islam, M.T.; Moniruzzaman, M.; Samsuzzaman, M.; Bais, B.; Arshad, H.; Muhammad, G. Square enclosed circle split ring resonator enabled epsilon negative (ENG) near zero index (NZI) metamaterial for gain enhancement of multiband satellite and radar antenna applications. *Results Phys.* **2020**, *19*, 103556. [CrossRef]
16. Simovski, C.R. On electromagnetic characterization and homogenization of nanostructured metamaterials. *J. Opt.* **2010**, *13*, 013001. [CrossRef]
17. Simovski, C.R. Material parameters of metamaterials (a review). *Opt. Spectrosc.* **2009**, *107*, 726–753. [CrossRef]
18. Arslanagić, S.; Hansen, T.V.; Mortensen, N.A.; Gregersen, A.H.; Sigmund, O.; Ziolkowski, R.W.; Breinbjerg, O. A review of the scattering-parameter extraction method with clarification of ambiguity issues in relation to metamaterial homogenization. *IEEE Antennas Propag. Mag.* **2013**, *55*, 91–106. [CrossRef]
19. Chen, X.; Grzegorczyk, T.M.; Wu, B.I.; Pacheco, J.; Kong, J.A. Robust method to retrieve the constitutive effective parameters of metamaterials. *Phys. Rev. E* **2004**, *70*, 016608. [CrossRef]
20. Szabó, Z.; Park, G.; Hedge, R.; Li, S.L. A unique extraction of metamaterial parameters based on Kramers–Kronig relationship. *IEEE Trans. Microw. Theory Tech.* **2010**, *58*,2646–2653. [CrossRef]
21. Varadan, V.V.; Ro, R. Unique retrieval of complex permittivity and permeability of dispersive materials from reflection and transmitted fields by enforcing causality. *IEEE Trans. Microw. Theory Tech.* **2007**, *55*, 2224–2230. [CrossRef]
22. Angiulli, G.; Versaci, M.; Calcagno, S.; Di Barba, P. Metamaterial unit cell characterization by using a multi-fidelity surrogate modelling approach. In Proceedings of the 19th International Symposium on Electromagnetic Fields in Mechatronics, Electrical and Electronic Engineering (ISEF), Nancy, France, 29–31 August 2019; pp. 1–2.
23. Angiulli, G.; Versaci, M.; Calcagno, S.; Di Barba, P. Quick retrieval of effective electromagnetic metamaterial parameters by using a Multi-fidelity Surrogate Modelling approach. *Eur. Phys. J. Appl. Phys.* **2020**, *90*, 20901. [CrossRef]
24. Yoo, S.; Lee, S.; Choe, J.H.; Park, Q.H. Causal homogenization of metamaterials. *Nanophotonics* **2019**, *8* , 1063–1069. [CrossRef]
25. Cao, Z.X.; Yuan, F.G.; Li, L.H. An automated phase correction algorithm for retrieving permittivity and permeability of electromagnetic metamaterials. *AIP Adv.* **2014**, *4*, 067115. [CrossRef]
26. Shi, Y.; Li, Z.Y.; Li, L.; Liang, C.H. An electromagnetic parameters extraction method for metamaterials based on phase unwrapping technique. *Waves Random Complex Media* **2016**, *4*, 417–433. [CrossRef]
27. Angiulli, G.; Versaci, M. An Analytic Continuation Algorithm for Recovering the Electromagnetic Parameters of Metamaterials. In Proceedings of the 2021 Photonics & Electromagnetics Research Symposium (PIERS), Hangzhou, China, 21–25 November 2021; IEEE: Piscataway, NJ, USA, 2021; pp. 2648–2652.
28. Hasar, U.C.; Muratoglu, A.; Bute, M.; Barroso, J.J.; Ertugrul, M. Effective constitutive parameters retrieval method for bianisotropic metamaterials using waveguide measurements. *IEEE Trans. Microw. Theory Tech.* **2017**, *65*, 1488–1497. [CrossRef]
29. Peiponen, K.E.; Vartiainen, E.M.; Asakura, T. *Dispersion, Complex Analysis and Optical Spectroscopy: Classical Theory*; Springer Science & Business Media: Berlin/Heidelberg, Germany, 1998; Volume 147.
30. Angiulli, G.; Versaci, M. Retrieving the Effective Parameters of an Electromagnetic Metamaterial Using the Nicolson-Ross-Weir Method: An Analytic Continuation Problem along the Path Determined by Scattering Parameters. *IEEE Access* **2021**, *9*, 77511–77525. [CrossRef]
31. Smith, D.R.; Vier, D.C.; Koschny, T.C.; Soukoulis, M. Electromagnetic parameter retrieval from inhomogeneous metamaterials. *Phys. Rev. E* **2005**, *71*, 036617. [CrossRef] [PubMed]
32. Markushevich, A.I. *Theory of Functions of a Complex Variable*, 2nd ed.; Chelsea Publishing Company: New York, NY, USA, 1985.
33. Peiponen, K.E.; Lucarini, V.; Vartiainen, E.M.; Saarinen, J.J. Kramers-Kronig relations and sum rules of negative refractive index media. *Eur. Phys. J. Condens. Matter Complex Syst.* **2004**, *41*, 61–65. [CrossRef]
34. Francisco, C.; Nabet, B. Numerical computation of the complex dielectric permittivity using Hilbert transform and FFT techniques. *J. Frankl. Inst.* **1999**, *336*, 53–64.
35. Palka, B.P. *An Introduction to Complex Function Theory*; Springer Science & Business Media: Berlin/Heidelberg, Germany, 1991.
36. Oppenheim, A.; Schafer, R.W. *Discrete Time Signal Processing*; Prentice Hall: Hoboken, NJ, USA, 2009.
37. Wegert, E. *Visual Complex Functions: An Introduction with Phase Portraits*; Springer Science & Business Media: Berlin/Heidelberg, Germany, 2012.
38. Lucarini, V.; Saarinen, J.J.; Peiponen, K.E.; Vartiainen, E.M. *Kramers-Kronig relations in Optical Materials Research*; Springer Science & Business Media: Berlin/Heidelberg, Germany, 2005.
39. Dirdal, C.A.; Skaar. J. Superpositions of Lorentzians as the class of causal functions. *Phys. Rev. A* **2013**,*88*, 033834. [CrossRef]
40. Groetsch, C.W. *Element of Applicable Functional Analysis*; Marcel Dekker: New York, NY, USA, 1980.
41. Chellappa, S.; Franchetti, F.; Puschel M. How to write fast numerical code: A small introduction. In *International Summer School on Generative and Transformational Techniques in Software Engineering*; Springer: Berlin/Heidelberg, Germany, 2007.